Thermal properties and residual strength after high temperature exposure of cement mortar using ferronickel slag aggregate

Ashish Kumer Saha[1*], Prabir Kumar Sarker[2], Vladimir Golovanevskiy [3]
[1]PhD student, School of Civil and Mechanical Engineering, Curtin University, Australia, Email: a.saha@postgrad.curtin.edu.au
[2]Associate Professor, School of Civil and Mechanical Engineering, Curtin University, Australia, Email: p.sarker@curtin.edu.au
[3] Professor, WA School of Mines: Minerals, Energy and Chemical Engineering, Curtin University, Australia, Email: V.Golovanevskiy@curtin.edu.au
*Corresponding author

Abstract

This study evaluates the thermal properties of cement mortar using by-product ferronickel slag (FNS) fine aggregate and its residual strength after high temperature exposure. Compressive strength of mortar increased when FNS was used up to 50% replacement of sand and then reduced with further increase of FNS. Volume of permeable voids (VPV) increased by 4% and 7% respectively for using 50% and 100% FNS fine aggregate. Thermal conductivity of mortar decreased from 2.34 W/m.K for using 100% sand to 1.65 W/m.K and 1.16 W/m.K for 50% and 100% FNS, respectively. Similarly, specific heat increased from 2.18 MJ/m^3.K to 2.43 MJ/m^3.K for 100% replacement of sand by FNS. These changes of VPV and thermal properties are attributed to the cavity of FNS particles, and their larger size and angular shape. Residual strengths of mortar after exposure to 800 ^{o}C were found marginally less for using FNS aggregate. This is attributed to the decrease of thermal conductivity of mortar by FNS. Overall, FNS aggregate showed improved thermal insulating properties and thermal mass of mortar without compromising compressive strength. Therefore, FNS can be considered for use as an energy efficient sustainable building material.

Keywords: Ferronickel slag; Heat capacity; Thermal conductivity; Thermal diffusivity; High temperature exposure; Air void; Sustainable building material.

1. Introduction

The annual growth of concrete production is estimated as 6% (Ghods et al, 2017). Demand of concrete is increasing at a high rate due to rapid infrastructure development in many countries like India and China. Production of concrete utilises an enormous amount of natural resources including sand as fine aggregate. Fine aggregate occupies about 25% to 30% volume of concrete and it contributes to the density and mechanical properties of concrete. Thus, it is essential to use good quality fine aggregate in concrete production. Natural sand is the most commonly used fine aggregate due to its suitable particle size, inertness, strength and thermal properties. However, good quality sand is not readily available in many countries of the world. As a result, excessive sand mining has occurred in different places that have caused significant damage to the aquatic environment (Preciso et al., 2012; Padmalal et al., 2008). Therefore, use of industrial by-products as replacement of natural sand can help protect the environment by value-added waste utilisation and conservation of natural resources. This study investigated the use of by-product FNS as a replacement of natural sand.

Thermal properties of concrete can play a significant role in sustainable infrastructure development. The stress distribution caused by temperature variation in structural elements can be significantly affected by thermal properties of concrete (Emborg, 2014). Temperature

variation may induce excessive tensile stress in concrete to cause cracks on surface and throughout cross-section. Mirzazadeh et al. (2016) conducted a study on the response of reinforced concrete at different temperature environments. It was found that low temperature delayed the crack propagation of reinforced concrete at a given load showing a correlation of cracks with temperature differential. Shen et al. (2016) showed that high temperature exposure can lead to an increase in autogenous shrinkage, and the authors developed a model to predict shrinkage of concrete due to different curing temperatures.

Optimisation of thermal insulation of concrete can help reduce the energy required for heating and cooling of buildings and thus reduce the use of fossil fuels (Liu et al. 2014). Mahila et al. (2007) showed that adequate thermal insulation could significantly reduce the operational cost of power plants. Lightweight aggregate and air-entraining agents are often used to improve thermal insulating properties of concrete. Borinaga-Trevino et al. (2013) studied the effects of different fine aggregates such as silica sand, limestone, electric arc furnace (EAF) slag and construction and demolition waste (CDW) on the thermal conductivity of cement mortar. The thermal conductivities of cement mortar using silica sand and EAF slag were found to be 2.1 W/mK and 1.5 W/mK, respectively. According to Kim et al. (2012), use of up to 1.5% air-entraining (AE) agent can significantly improve the thermal insulation of concrete. The experimental study showed that there was 52% to 55% reduction of thermal conductivity due to the use of 1.5% AE agent that increased porosity. Alengaram et al. (2013) showed that oil palm shell foamed concrete reduced thermal conductivity of concrete by 39% as compared to control concrete. Ramírez et al. (2013) showed by experimental results that replacement of 80% natural aggregate by lightweight recycled aggregate provided 65% reduction in thermal conductivity due to the increase of porosity of concrete. Similarly, use of 30% hollow glass spheres as coarse aggregate was found to reduce thermal conductivity of concrete by 43% (Yun et al. 2013). Thus, use of porous aggregate or creation of air voids in concrete improved thermal insulation by reducing thermal conductivity. However, both light-weight aggregates and air voids can result in a significant reduction of strength due to reduced density and increased porosity of concrete (Won et al. 2011).

Thermal conductivity of concrete and mortar also depends on the moisture content because the thermal conductivity of water is twenty-five times higher than that of air (Morabito, 1989). Del Coz Díaz et al. (2013) studied the effects of density and relative humidity on thermal properties of light-weight aggregate concrete. Steiger and Hurd (1978) found that 1% increase in specific weight of concrete due to water absorption resulted in 5% increase of its thermal conductivity. Some other factors that are shown to influence thermal conductivity of concrete are volume of cement (Örüng, 1996), aggregate characteristics, mineral admixtures (Fu and Chung, 1997), and temperature (Metha and Monteiro, 2006). Thermal conductivity of concrete is also shown to increase with the increase of density (Institution of Structural Engineers, 1987; Ashworth and Ashworth, 1991; Demirboga and Kan, 2012). Sayadi et al. (2016) proposed an equation to predict thermal conductivity of a very light-weight foamed concrete as a function of the density of concrete and the volume of expanded polystyrene. It is noteworthy that the voids content of concrete have a significant effect on thermal conductivity. A numerical investigation by Del Coz Díaz (2010) showed that the heat transfer through floors made using hollow concrete blocks could be significantly different for different shape and number of the layer of blocks.

Prolonged exposure to elevated temperatures can cause explosive spalling of concrete and lead to structural failures (Won et al. 2011). When exposed to heat, the binder matrix initially loses the physically bound water at about 100 °C to 150 °C. Decomposition of portlandite and evaporation of chemically bound water occurs between 500 °C and 550 °C.

Further increase in temperature leads to the decomposition of calcium carbonate at about 750 °C to 800 °C, and results in a major strength loss (Yüzer et al., 2004; Esteves, 2011; Kodur, 2014). Different techniques have been adopted to improve the resistance of concrete against high temperature exposure. Supplementary cementing materials (SCM) such as ground blast furnace slag (GGBFS), fly ash and metakaolin may show improvement of residual strength up to a temperature of 400 °C due to the pozzolanic reaction of SCM (Papayianni & Valliasis, 2005; Li et al., 2012). Use of polyvinyl alcohol (PVA) fibres with low melting point improves fire endurance of concrete by reducing the vapour pressure generated by heat (Soleimanzadeh & Mydin, 2012).

Since aggregates generally occupy about 70% to 80% volume of concrete, thermal properties of aggregate have a significant influence on the thermal properties of concrete. Thermal properties of concrete eventually influence its behaviour when exposed to high temperature heat. According to Topçu & Işıkdağ (2007), lightweight aggregate exhibited excellent resistance to high temperature exposure due to the reduction of thermal conductivity of concrete. Similarly, Zhang et al. (2000) showed that concretes with lightweight aggregate exhibit remarkable thermal resistance over concrete using normal weight aggregates, while subjected to an elevated temperature of up to 600 °C. According to Kodur & Sultan (2003), carbonate aggregate exhibited higher fire resistance as compared to siliceous aggregate due to lower thermal conductivity. In addition, Kodur et al. (2003) experimentally showed higher specific heat of carbonate aggregates than siliceous aggregates that prevented spalling of concrete using carbonate aggregate at high temperature. Kong & Sanjayan (2010) showed that concrete using smaller size aggregates exhibited more cracking than concrete with larger aggregates due to thermal incompatibility between the binder matrix and aggregate. Similarly, Pan et al. (2012) showed that concrete with 10 mm aggregates suffered from more spalling than concrete with 14 mm aggregates. This is because larger aggregate creates an elongated fracture process zone to facilitate the escape of vapour pressure. Therefore, the type and size of aggregates showed significant effects on thermal properties of concrete and its response after exposure to high temperature.

The effects of using FNS fine aggregate on thermal properties of cement mortar are presented in this paper. The FNS used in this study is a by-product of the smelting of garnierite nickel ore and was sourced from SLN, New Caledonia. It has been estimated that about 12 tonnes of FNS is generated as by-product in production of 1 tonne ferronickel alloy. Thus, a huge quantity of FNS is available for use as a construction material. A water cooling method was used to granulate the molten slag. As shown in previous studies (Saha & Sarker, 2016), FNS aggregate consists of high density particles and it can improve compressive strength of concrete when used as a partial replacement of sand. However, full replacement of sand by FNS reduced compressive strength (Saha & Sarker, 2017b, 2018a). Since thermal properties of a matrix are dependent of the fine aggregate filler, it is essential to evaluate the thermal properties of mortar using FNS aggregate and its effect after the mortar is exposed to high temperature heat. There are no previous studies where thermal properties of cement mortar containing FNS aggregate were evaluated. Therefore, this study was conducted in order to evaluate the thermal properties of mortar using FNS aggregate. Mortar specimens were cast using FNS aggregate as different volume percentage replacements of sand. Various properties such as density, compressive strength, thermal conductivity, thermal diffusivity, specific heat, permeable voids and resistance to elevated temperature of mortar specimens were determined. The effects of FNS aggregate on mortar properties were further investigated by scanning electron microscope (SEM) images of the aggregates and mortars.

2. Materials and methods

2.1 Materials

Ordinary Portland cement (OPC) was used as the binder for casting of mortar specimens. The specific surface area and density of OPC were 337 m^2/kg and 3.15 g/cm^3, respectively. Locally available natural silica sand and ferronickel slag (FNS) were used as fine aggregate. The chemical compositions of OPC and FNS, as determined by X-ray fluorescence (XRF) analysis, are given in Table 1. It can be seen that the main constituents of FNS are silicon, magnesium and iron. Leaching of heavy metals from concrete specimens containing 100% FNS fine aggregate was studied previously and the results are available in literature (Saha and Sarker, 2017a). It was found that the leaching of heavy metals were much less than the recommended limits of the United States Environmental Protection Agency (US EPA, 2009). Therefore, the use of FNS aggregate in concrete was found environmentally safe in terms of the leaching of heavy metals.

Table 1. Chemical compositions of OPC and FNS (mass percentage).

Chemical composition	OPC	FNS
SiO_2	20.29	53.29
Al_2O_3	5.48	2.67
Fe_2O_3	2.85	11.9
MgO	1.24	31.6
SO_3	2.49	-
CaO	63.11	0.42
Na_2O	0.29	0.11
K_2O	0.45	-
Cr_2O_3	0.02	1.08
P_2O_5	0.17	-
SrO	0.05	-
TiO_2	0.27	-
Mn_2O_3	0.08	-
ZnO	0.04	-
NiO	-	0.1
Co_3O_4	-	0.01
loss on ignition	3.39	-

The physical properties of aggregates are given in Table 2. It can be seen that FNS has higher specific gravity and fineness modulus as compared to sand. Physical appearances of the aggregates are shown in Fig. 1. FNS aggregate is dark in colour and consists of particles of different sizes. On the other hand, sand consisted of round particles of uniform size. Additionally, presence of some cavities can be visible in the FNS particles, as shown in Fig. 1. Furthermore, the SEM images of FNS and sand particles are shown in Fig. 2. It can be seen that the microstructure of FNS particles is relatively porous as compared to that of natural sand. The large cavity is shown in Fig. 1(a) and the microstructural pores are shown in Fig. 2(a) are believed to have formed during the rapid cooling of molten FNS to produce granulated

166 particles. Particle size distributions of the aggregates are presented in Fig. 3 along with the
167 upper and lower limits recommended by AS 2758.1 (2014). It can be seen that FNS has higher
168 fractions of coarse particles as compared to natural sand. The maximum particle sizes of sand
169 and FNS aggregate were 1.18 mm and 4.75 mm, respectively. The grading curves show that
170 the mix of 50% FNS with 50% sand provided a well-grading of the fine aggregate.

171 **Table 2.** Physical properties of aggregates.

Materials	Specific gravity	Fineness modulus	Water absorption (%)
Sand	2.10	1.95	0.35
Ferronickel slag (FNS)	2.78	4.02	0.42

172

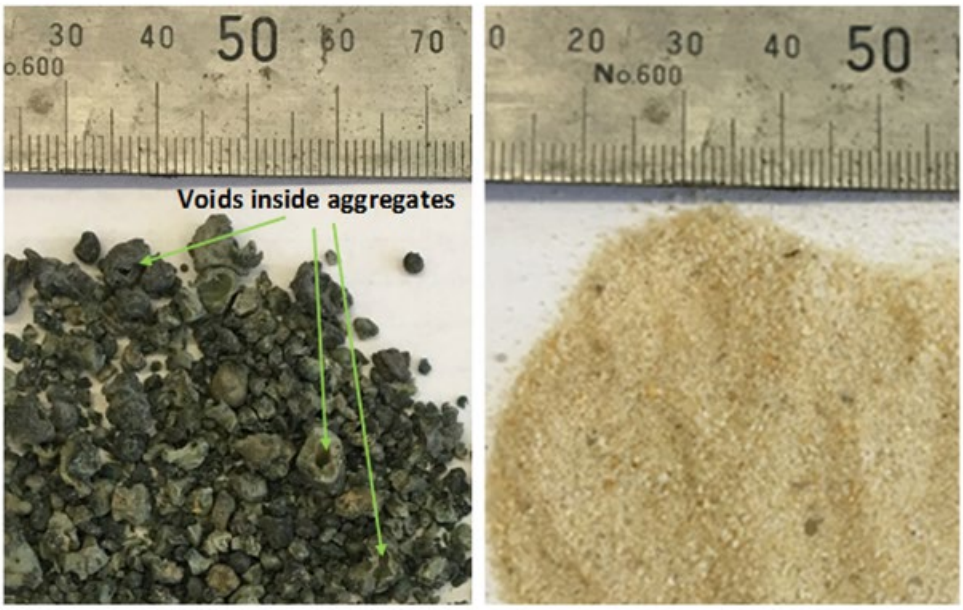

(a) FNS (b) Sand

173

174 **Fig. 1.** Physical appearance of the aggregates.

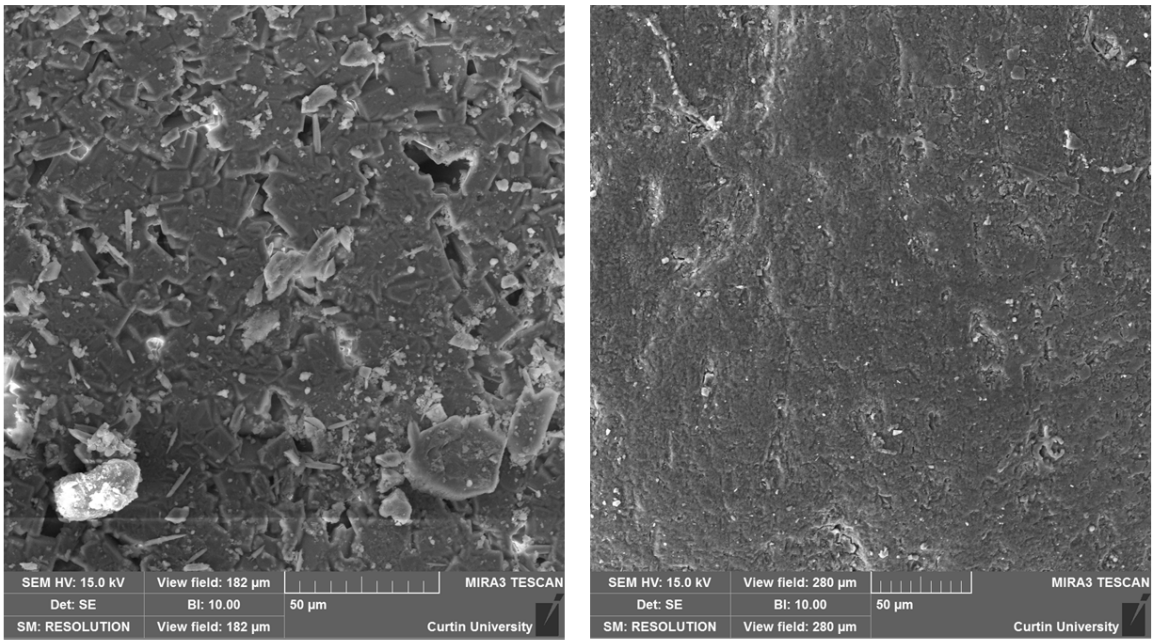

(a) FNS (b) Sand

Fig. 2. Microstructures of FNS and sand.

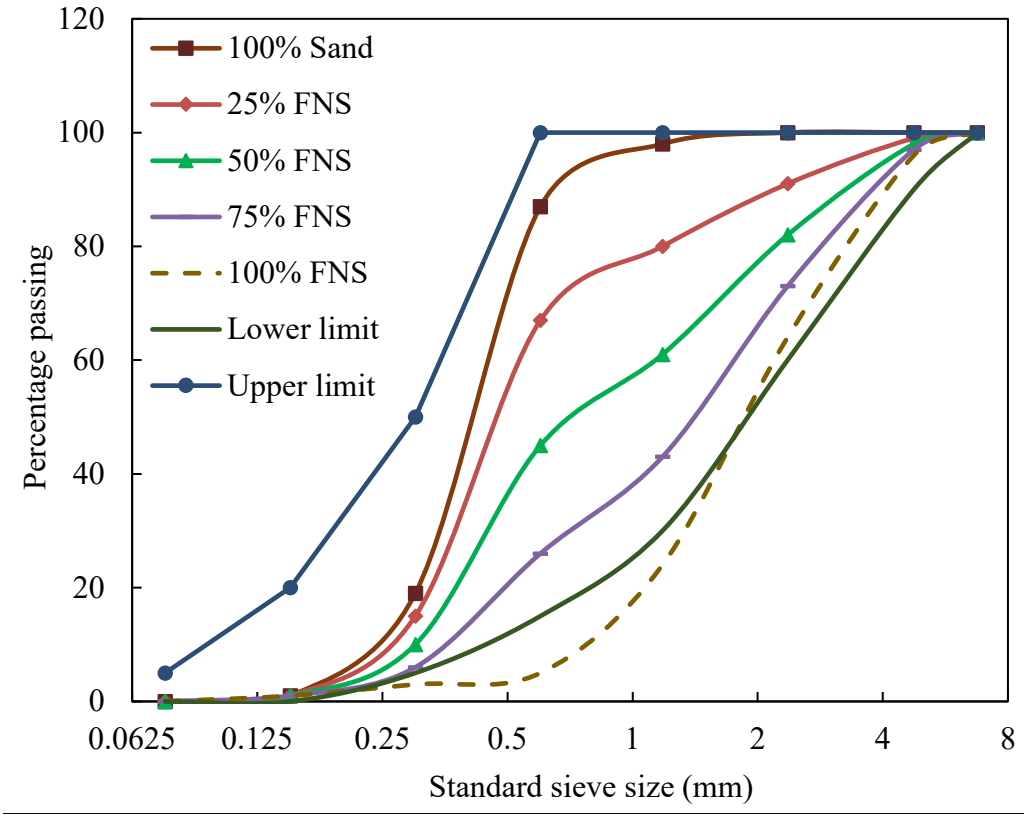

Fig. 3. Grain size distribution of sand, FNS and recommended limits of AS 2758.1 (2014).

2.2 Sample preparation and test methods

The mortar mixtures were mixed according to the guidelines of Australian Standard AS 2701 (2001). Mix proportions are given in Table 3. Cement content of the mixture was 450 kg/m^3 and water to cement ratio was 0.5. Fine aggregate to binder ratio was 2.75. Sand was replaced by FNS from 25% to 100% volume of the fine aggregate. Five mortar mixtures were studied and the reported results are the average values for three identical specimens. The mixtures are designated by volume percentage of FNS. Fifty-mm cube specimens were cast for compressive strength tests of mortars. The specimens were demoulded at 24 hours after casting and then cured for 28 days. Compressive strength was determined by loading the specimens at a rate of 0.33 MPa/sec. The density and volume of permeable voids (VPV) were determined using mortar cube specimens. VPV was determined from saturated surface dry (SSD) and oven dry masses of the specimens according to ASTM C 642 (2006). SEM images of sand, FNS and the mortar specimens were used to understand the effect of FNS on mortar properties. SEM was conducted by backscatter electron beam with an accelerating voltage of 10 kV and a constant working distance.

Table 3. Mix proportions of mortar.

Sample ID	OPC (kg/m^3)	Fine aggregate (kg/m^3)		Water (kg/m^3)	W/C
		Sand	FNS		
PC-FNS0	450	1250	0	275	0.50
PC-FNS25	450	935	415	275	0.50
PC-FNS50	450	625	825	275	0.50
PC-FNS75	450	310	1240	275	0.50
PC-FNS100	450	0	1655	275	0.50

Cylindrical specimens of 100 mm diameter and 200 mm height were cast to determine the thermal properties. The cylinders were cut into 30 mm thick discs after curing in water for 28 days. The specimens were then oven-dried at 105 °C for 24 hours, cleaned with a soft synthetic-fibre brush and kept in an air-tight container to prevent contamination by airborne dust. Thermal properties analyser Hot Disk TPS 2200 instrument and transient plane source (TPS) technique developed by Gustafsson (1991) was used for the test. Some of the main advantages of using the TPS technique include its inherent ability to measure thermal conductivity and thermal diffusivity in the same measurement step and the small temperature gradients necessary for the measurements (Bouguerra et al., 1997). The latter quality of the TPS method is particularly useful for potentially temperature-affected materials. In our research, all the measurements were conducted at 22 ± 0.5 ºC temperature and the instrument-induced temperature gradient was limited to 4.2 ºC. Given the 30 mm thickness of test samples and to ensure no influence of the specimen/specimen holder boundary conditions, the depth of heat flow penetration was limited to 20.0 mm. The experimental setup is shown in Fig. 4.

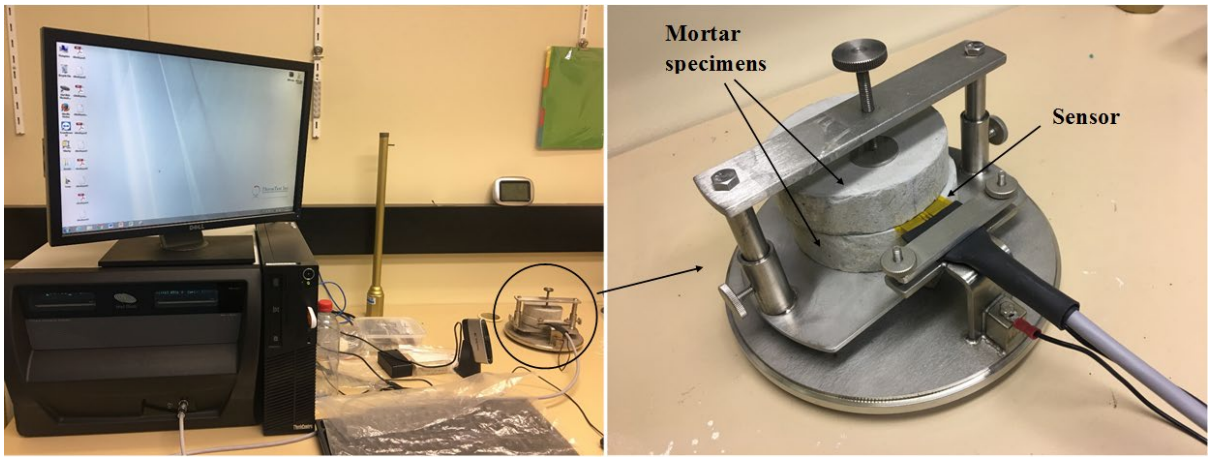

Fig. 4. Experimental set up to determine thermal properties. Note: sample holder cover removed for the photograph.

The test samples were cut in a single cutting step using a rotary masonry saw with a diamond-tipped blade. This ensured that surface of the samples was flat and smooth. Referring to Fig. 4, the sensor of the TPS instrument was positioned in-between the duplicate samples and the assembly was then compressed with the hold-down screw. Good mechanical contact between the TPS sensor and the surfaces of the duplicate specimens ensured good thermal contact and this minimized any potential influence of surface resistance on the results. This approach to minimise thermal contact resistance has been a widely accepted practice (Berman, 1956; Thomas and Probert, 1970; Williamson and Majumdar, 1992). Additionally, Gustaffson et al. (1986) found that the influence of thermal contact resistances in the transient thermal measurements appeared only for a short time period at the beginning of the measurement, where it presented as a constant temperature difference which could be easily recognised by the thermal analysis software. In our research, the constant temperature difference due to thermal contact resistance at the beginning of all measurements was of the order of 0.1 mK and appeared for less than 5 ms only (at the total measurement time of 80 s). It was recognised and separated from the transient temperature increase in the bulk material by thermal analysis software.

The residual strengths after exposure to elevated temperature were evaluated by heating the 50 mm cube specimens in an electric furnace. The samples were heated to 200 °C, 400 °C, 600 °C and 800 °C with a temperature increment rate of 5 °C per minute. After reaching the designated temperature level, the temperature was kept constant for two hours. The samples were then cooled down to room temperature naturally by opening the door of the furnace. The mass and compressive strength were determined after cooling down the specimens to room temperature.

3. Results and discussion

3.1 Density of hardened mortar

The average densities of the hardened mortars in saturated surface dry (SSD) condition and oven-dry condition are presented in Table 4. It can be seen that the SSD density varied in a range of 1945 kg/m^3 to 2361 kg/m^3.

Table 4. Density of hardened mortar.

Mix ID	SSD density (kg/m^3)	Oven-dry density (kg/m^3)
PC-FNS0	1945	1735
PC-FNS25	2060	1834
PC-FNS50	2143	1897
PC-FNS75	2258	1961
PC-FNS100	2361	2023

As shown in Fig. 5, density of the mortar increased linearly with the increase of FNS content. This is due to the higher particle density of FNS aggregate than sand. It can also be seen that the densities of the oven-dry samples were 11% – 15 % less than the SSD samples. The differences between the oven-dry and SSD densities of mortars PC-FNS0, PC-FNS25, PC-FNS50, PC-FNS100 and PC-FNS100 were 210 kg/m^3 226 kg/m^3, 248 kg/m^3, 297 kg/m^3 and 338 kg/m^3, respectively. Therefore, moisture content of mortar specimens gradually increased with the increase of FNS aggregate. While air-dry samples were used for the compressive strength tests, the samples used for thermal conductivity tests were in oven-dry condition in order to avoid the interference of the water content (Sengul et al. 2011).

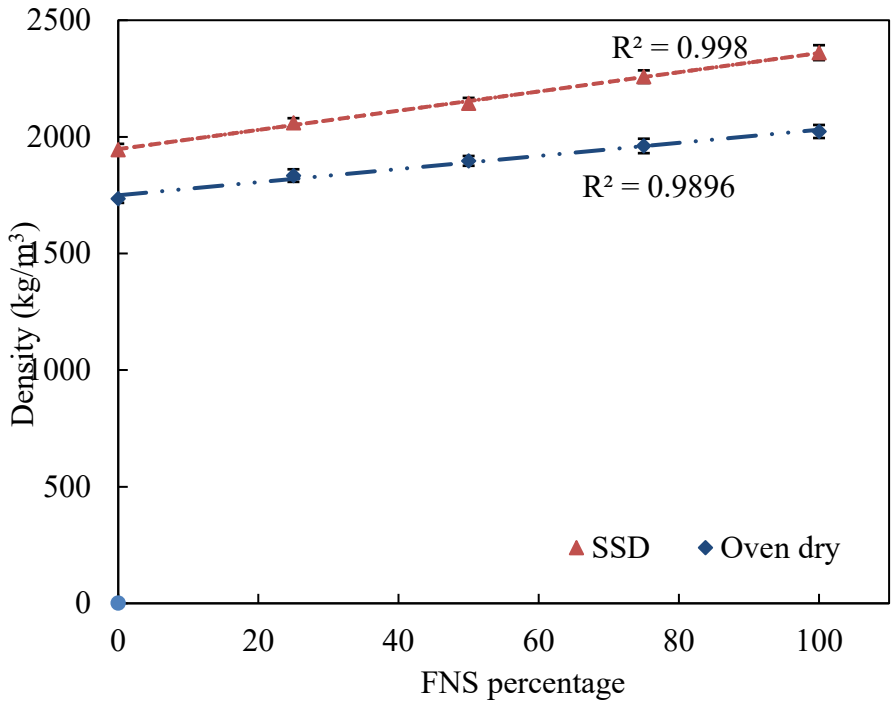

Fig. 5. Relationship between density and the FNS content.

3.2 Compressive strength

The compressive strength results are shown in Fig. 6. As expected, compressive strength mortar increased significantly between 7 days and 28 days, while it became almost steady between 28 days and 56 days of age. This trend was consistent for all the five mortar mixtures. As in conventional mortar using natural sand, majority of the compressive strength development of mortars using FNS aggregate occurred during the first 7 days of curing. It can be seen that the 7-day compressive strengths of mortars PC-FNS0, PC-FNS25, PC-FNS50, PC-FNS75 and PC-FNS100 were 73%, 78%, 74%, 70% and 66% of their 56-day strengths, respectively. Furthermore, the 28-day strengths of mortars PC-FNS0, PC-FNS25, PC-FNS50, PC-FNS75 and PC-FNS100 were 96%, 97%, 96%, 96% and 97% of their 56-day strength, respectively. Thus, the strength development after the age of 28 days was relatively low.

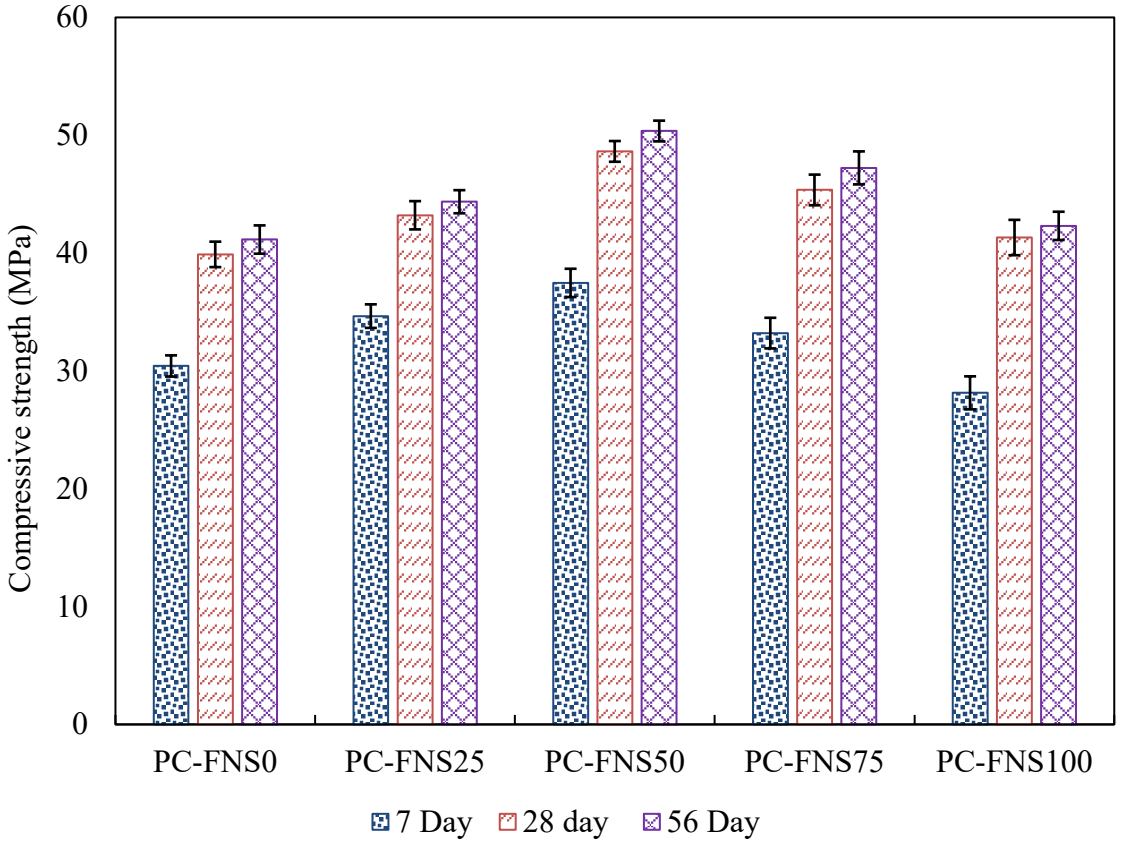

Fig. 6. Compressive strength of the mortar samples.

It can also be seen that compressive strength at any particular age improved with the increment of FNS up to 50% replacement of sand. However, further increase of FNS content resulted in decline of compressive strength. The 28-day mortar compressive strengths were 40 MPa, 43 MPa, 48 MPa, 45 MPa and 41 MPa for using 0%, 25%, 50%, 75% and 100% FNS aggregate, respectively. Therefore, the strength increments were 8%, 21%, 13% and 3% for using 25%, 50%, 75%, and 100% FNS, respectively. It is usual for concrete and mortar to show higher compressive strength for higher density due to better particle packing and lower voids content (Güneyisi et al. 2016; Bogas et al. 2015). Thus, the increase of mortar strength by using FNS aggregate is attributed to the increase of the density of specimens. As shown in Fig. 3, the combination of 50% sand with 50% FNS resulted in a well-graded aggregate. However, the FNS contents above 50% increased the voids content due to their angular shape and larger size.

This caused a decline in the compressive strength of mortar using FNS contents of 75% and 100%. Similar effect of FNS fine aggregate content was also observed on the compressive strength of concrete specimens (Saha & Sarker 2017a, 2018b).

3.3 Volume of permeable voids

In order to evaluate the porosity of the samples, the volume of permeable voids (VPV) was determined. The test measures the ease with which water can penetrate into a mortar or concrete sample. The combination of air voids, capillary pores, gel pores and micro-cracks is determined by the VPV (Andrews-Phaedonos, 2008).

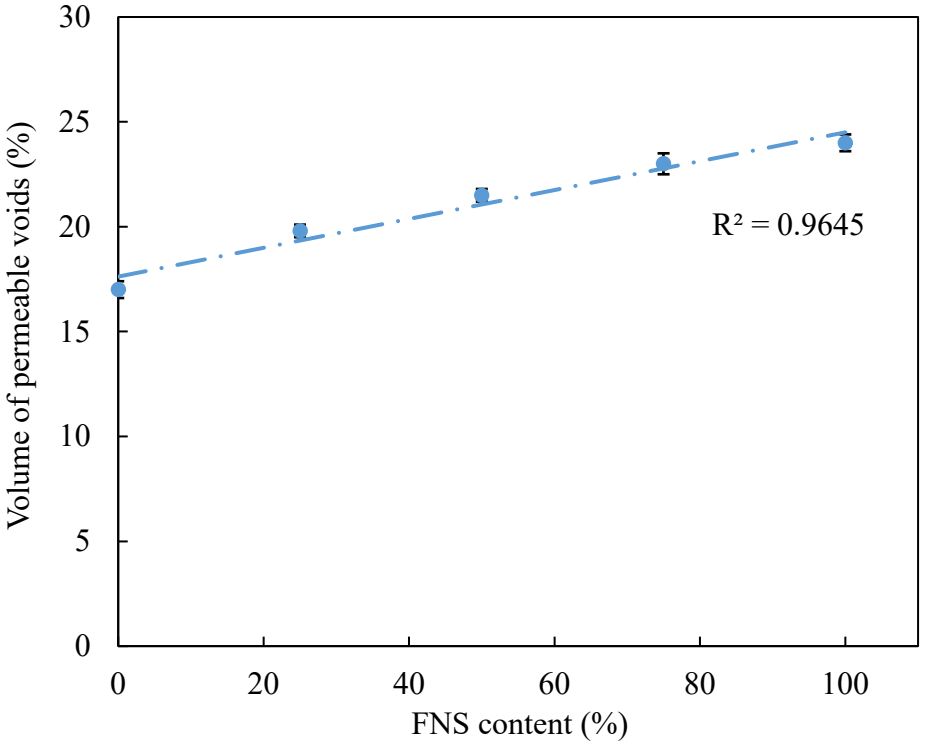

Fig. 7. Relationship between VPV and FNS aggregate content.

The experimental results of VPV are shown in Fig. 7. It can be seen that VPV of mortar increased with the increase of FNS content. VPV of the specimens PC-FNS0, PC-FNS25, PC-FNS50, PC-FNS75 and PC-FNS100 were 17%, 20%, 21%, 23%, and 24%, respectively. The increase of VPV indicates an increase of the porosity of mortar with the increase of FNS content. For instance, VPV of mortar increased by 4% and 7% for using 50% and 100% FNS aggregate, respectively, as compared to using 100% sand.

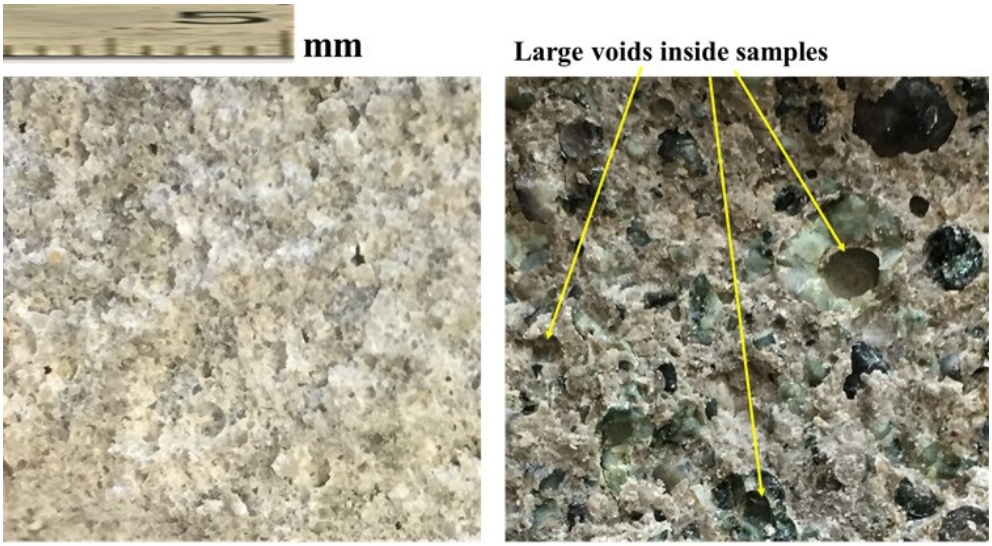

(a) PC-FNS0 (b) PC-FNS100

Fig. 8. Imges of mortar cross section after 28 days of curing (10 × magnification).

Magnified views of the cross-section of mortar specimens and SEM images of the microstructure were investigated in order to further understand the increase of porosity by FNS. It can be seen from the magnified view of the cross-section in Fig. 8 that there were relatively large air voids in the cross-section of specimen PC-FNS100 as compared to that of PC-FNS0. These air voids are produced by the cavities of FNS particles, as shown in Fig. 1(a). The SEM images of Fig. 9 shows that the microstructures of the binder matrix were very similar in the specimens of PC-FNS100 and PC-FNS0. Therefore, the increase of VPV or porosity in the specimens using FNS aggregate is contributed mostly by the cavities and micropores of the FNS particles shown in Fig. 1(a) and 2(a), respectively. Overall, the increase of porosity is attributed to the presence of voids in FNS particles and the relatively large size and angular shape of the particles.

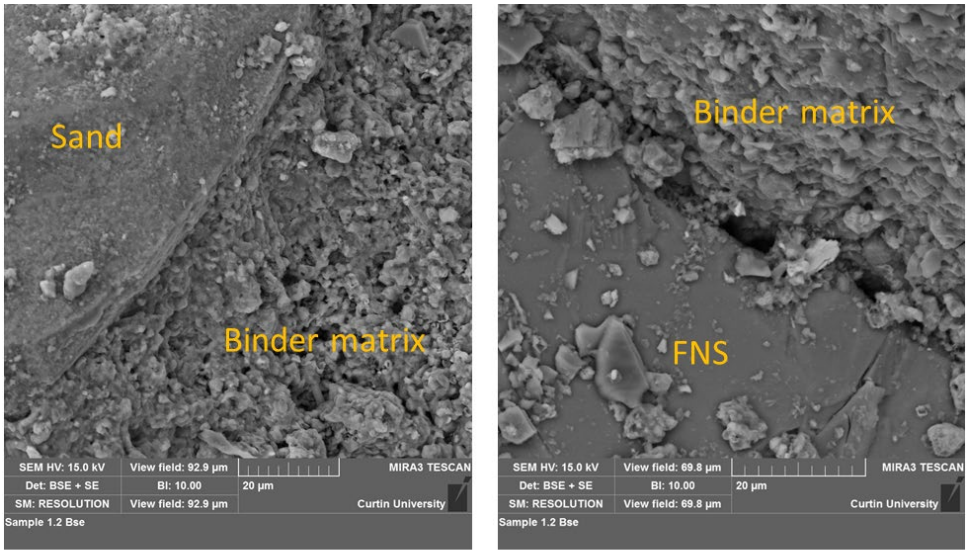

(a) PC-FNS0 (b) PC-FNS100

Fig. 9. SEM images of mortar cross section after 28 days of curing.

3.4 Thermal properties

The thermal properties of hardened mortar specimens are given in Table 5. The thermal conductivity values of mortars PC-FNS0, PC-FNS25, PC-FNS50, PC-FNS75 and PC-FNS100 were 2.34 W/m·K, 1.58 W/m·K, 1.65 W/m·K, 1.36 W/m·K and 1.16 W/m·K, respectively. The results show that thermal conductivity exhibited a decreasing trend with the increase of FNS content despite the higher specific gravity of FNS than sand. It can be noted from Table 2 that the specific gravities of FNS and sand were 2.78 and 2.10, respectively. A decrease of thermal conductivity by the use of high-density EAF slag was also reported by Borinaga-Trevino et al. (2013). The specific gravities of sand and EAF slag were 2.65 and 3.82, and the corresponding thermal conductivities of cement mortars were 2.1 W/m·K and 1.5 W/m·K, respectively. The decreasing trend of thermal conductivity with the increase of FNS is attributed to the increase of VPV, as shown in Fig. 7. The large cavities (Fig. 8) and micropores (Fig. 2) of FNS particles increased the porosity of mortar. This increase of air voids inhibited the heat flow that reduced the thermal conductivity of the specimens. The effect of the voids in FNS particles on thermal conductivity was found to be significant since 60% volume of the mortar is occupied by aggregate.

Table 5. Thermal properties of mortar samples.

Mix ID	Thermal conductivity, W/m·K	Thermal diffusivity, mm^2/s	Specific heat, $MJ/m^3 \cdot K$
PC-FNS0	2.34	1.07	2.18
PC-FNS25	1.58	0.79	2.00
PC-FNS50	1.65	0.74	2.24
PC-FNS75	1.36	0.61	2.26
PC-FNS100	1.16	0.48	2.43

In addition to thermal conductivity, thermal diffusivity and heat capacity are two other important parameters defining the heat transfer properties of a material. Thermal diffusivity represents the rate of heat transfer through the material and heat capacity or specific heat is the ratio of thermal energy absorbed or lost by a material to the corresponding temperature change (Lightfoot et al., 1960; Resnick and Halliday, 1966). As given in Table 5, thermal diffusivity values of the mortars PC-FNS0, PC-FNS25, PC-FNS50, PC-FNS75 and PC-FNS100 were 1.07 mm^2/s, 0.79 mm^2/s, 0.74 mm^2/s, 0.61 mm^2/s and 0.48 mm^2/s, respectively.

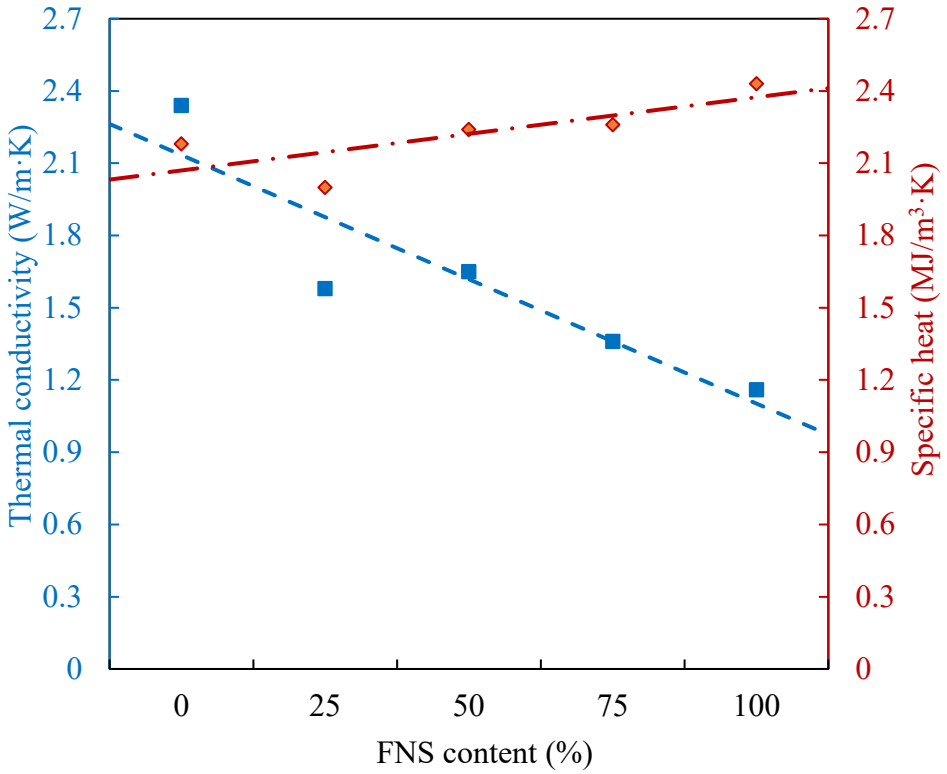

Fig. 10. Variation of thermal conductivity and specific heat with FNS content.

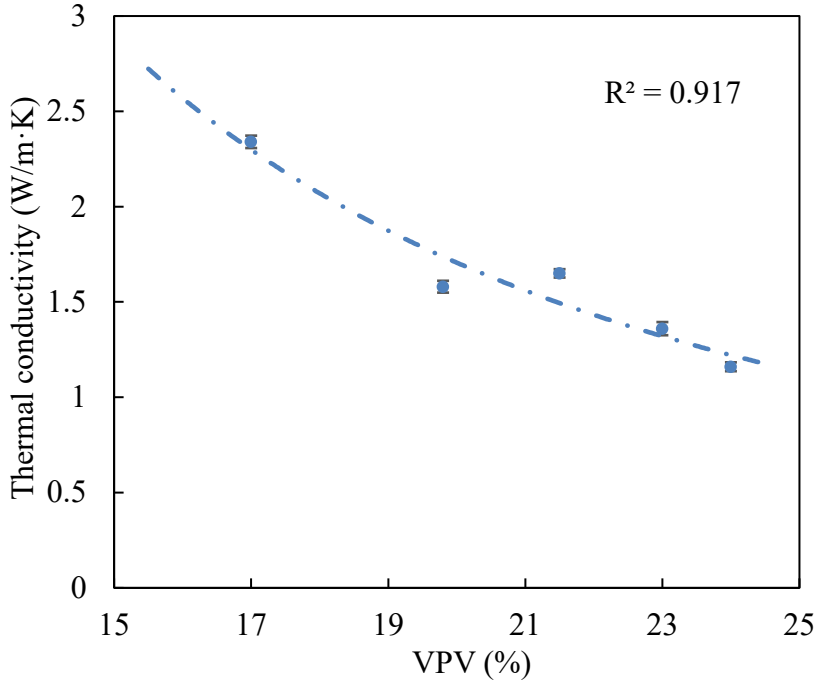

Fig. 11. Variation of thermal conductivity with VPV.

346 The variation of thermal conductivity and specific heat with FNS content are shown in Fig. 10.
347 It can be seen that there was a gradual decrease in thermal diffusivity with the increase of FNS
348 aggregate due to the increment of internal pores inhibiting the heat flow. The increase in
349 porosity of the samples has also been reflected in the corresponding increase in their heat
350 capacity values. Specific heat is the amount of heat required to increase temperature of a sample
351 to a unit value and there was a gradual increment of air voids with the increase of FNS content
352 in mortar samples, as shown in Fig. 7. As a result, a higher amount of heat transfer was required
353 for the FNS mortar samples to raise the temperature. This is the reason for a proportional
354 relationship between specific heat and FNS content as shown in Fig. 10.

355 Furthermore, in order to evaluate the relationship between the thermal conductivity and
356 porosity of the samples, the thermal conductivity values are plotted against the VPV, as shown
357 in Fig. 11. It can be seen that thermal conductivity gradually decreased with the increase of
358 VPV. A Power regression analysis between these two parameters shows a good correlation
359 with a degree of determination (R^2) value of 0.92. This confirms the hypothesis that the
360 presence of air voids was the primary reason behind low thermal conductivity of mortars
361 containing FNS aggregates despite their higher density as compared to the control samples.

362 ***3.5 Residual properties of mortar after exposure to elevated temperature***

363 *3.5.1 Visual observation*

364 The mortar specimens were visually inspected before and after the exposure to elevated
365 temperature. The samples were exposed to four different peak temperatures from 200 °C to
366 800 °C. The typical photographs of mortar specimens PC-FNS0, PC-FNS50 and PC-FNS100
367 taken after cooling down to room temperature from different temperature exposures are
368 presented in Fig. 12, Fig. 13 and Fig. 14, respectively.

369 It can be seen from Fig. 12 (a) that an exposure to 200 °C did not cause any noticeable
370 damage to the control specimen. Referring to Fig. 13 (a) and Fig. 14 (a), the PC-FNS50 and
371 PC-FNS100 samples were also free of any visual damage. Similarly, there was no crack in the
372 specimens containing 25% and 75% FNS aggregate exposed to 200 °C. After exposure to 400
373 °C, some fine cracks were noticeable on the surface of the PC-FNS0 samples, as shown in Fig.
374 12 (b). Similar thin cracks were consistently seen in all the five types of mortar specimens. For
375 instance, the cracks of the specimens using 50% FNS and 100% FNS aggregate are shown in
376 Fig. 13 (b) and Fig. 14 (b), respectively.

377

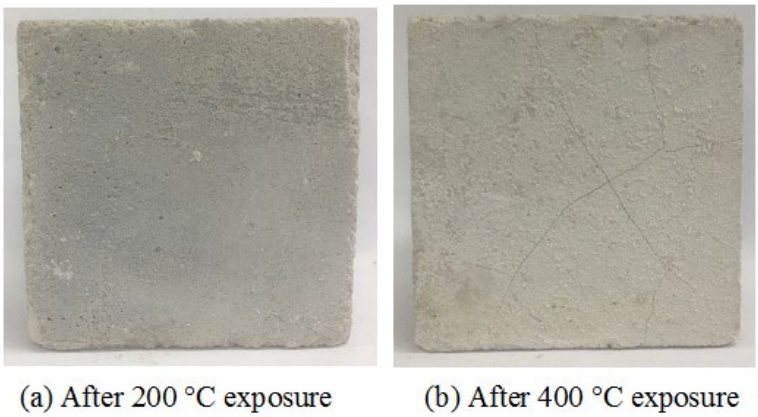

Fig. 12. Appearance of PC-FNS0 specimens after elevated temperature exposure.

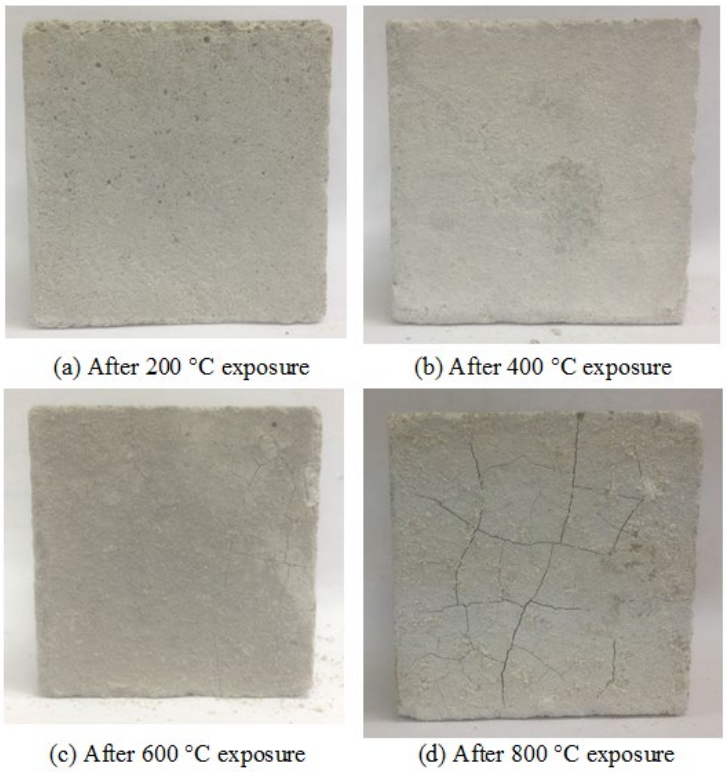

Fig. 13. Appearance of PC-FNS50 samples after elevated temperature exposure.

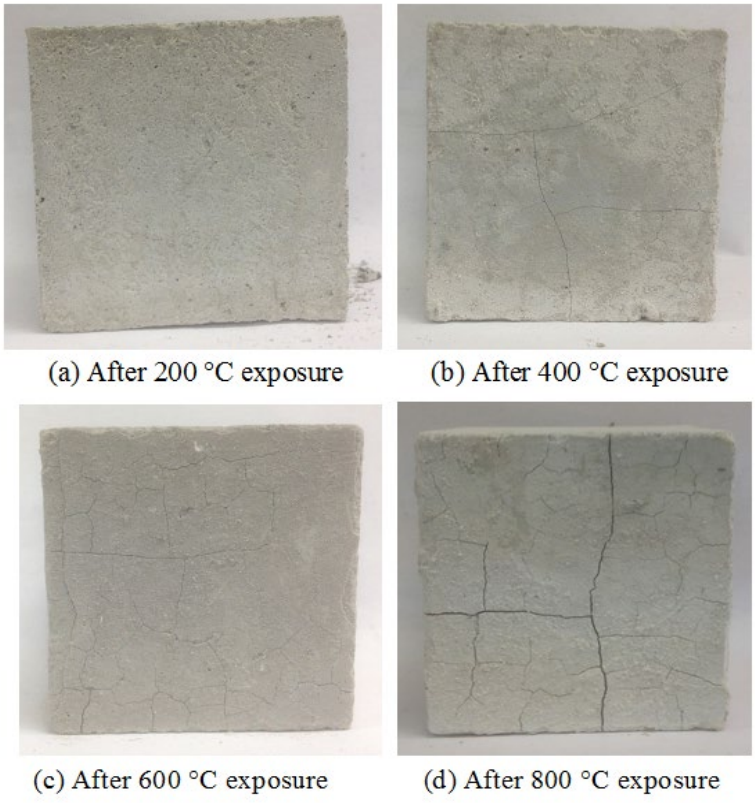

Fig. 14. Appearance of PC-FNS100 samples after elevated temperature exposure.

After 600 °C exposure, the cracks on the surface of specimens PC-FNS0, PC-FNS50 and PC-FNS100 can be seen in Fig. 12 (c), Fig. 13 (c) and Fig. 14 (c), respectively. It can be seen that the number of cracks increased in all three cases as compared to Figs. 12 (b), 13 (b) and 14 (b). Nevertheless, at this temperature, similar types of cracks were seen on surface of the specimens using different volumes of FNS aggregate. Finally, after the exposure to 800 °C, all mortar specimens exhibited significantly increased number of cracks on the surface as shown in Figs. 12 (d), 13 (d) and 14 (d). No spalling was observed in the specimens at this very high-temperature exposure of 800 °C for two hours. It was shown previously that mortar and concrete with high-density aggregates could experience explosive spalling at high-temperature exposure due to high vapour pressure (Ma et al., 2015). However, no such spalling was not observed in the mortar specimens containing up to 100% FNS aggregate. This is considered to be due to the higher porosity of the specimens using FNS aggregate that eased the release of internal vapour pressure. For this reason, excessive cracking or spalling was not observed in the specimens using FNS aggregate in spite of the reduced thermal conductivity of mortar. The cracks in both types of specimens were similar and are considered to have occurred due to the temperature differential, especially in the cooling stage.

3.5.2 Change of mass by exposure to high temperature

Mass of the samples was recorded before and after the elevated temperature exposure, and the percentages of mass change at different temperatures were calculated. The results are shown in Fig. 15.

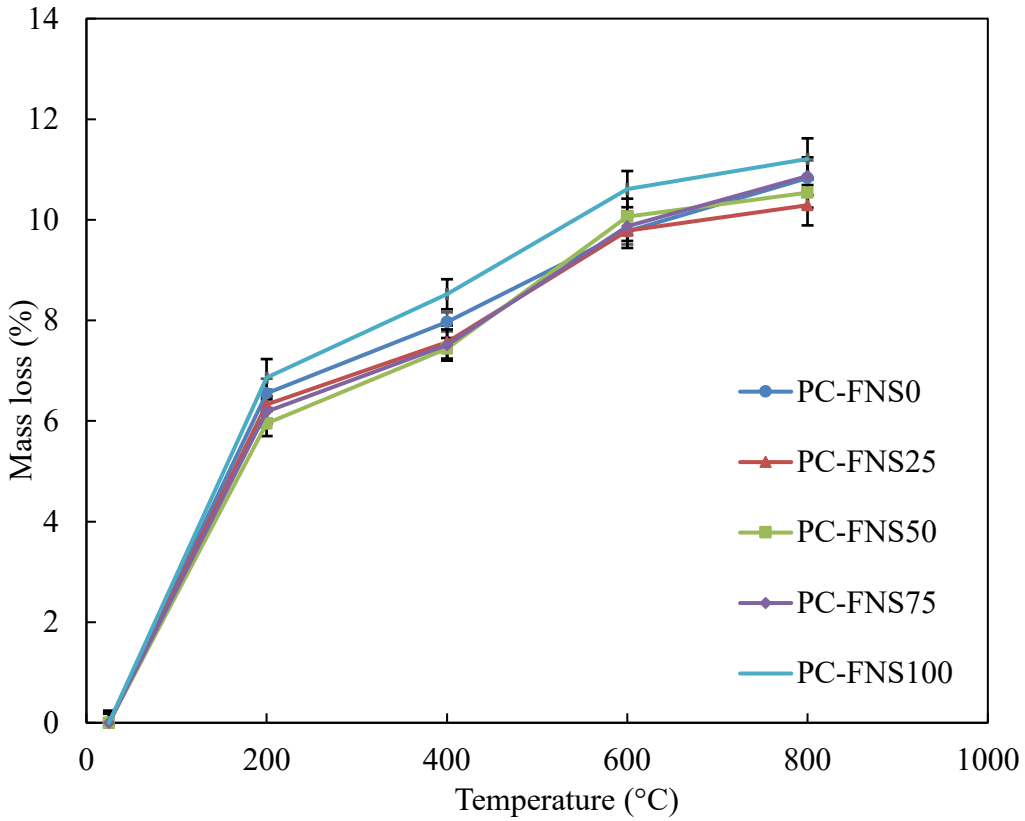

Fig. 15. Mass loss due to elevated temperature exposure.

It can be seen from Fig. 15 that the specimens exhibited a significant mass loss after exposure to 200 °C. Afterwards, the mass loss increased at a slower rate for exposure to 400 °C. Then, the mass loss again increased at a higher rate for exposure to 600 °C. Finally, from 600 °C to 800 °C, the mass loss increased at a declined rate. The reason for the substantial mass loss from room temperature to 200 °C is primarily due to the loss of physically bound water from the binder matrix. It is usually known that cement paste loses most of the physically bound water at temperatures up to 150 °C (Esteves, 2011). This corresponds to the significant mass loss observed in all the specimens up to 200 °C. The mass loss between 400 °C and 600 °C was primarily associated with the decomposition of portlandite or $Ca(OH)_2$ in the binder matrix. Decomposition of portlandite resulted in the escape of moisture from the samples and caused a notable mass loss. Besides, it can be seen that there was no noticeable variation of mass due to use of FNS aggregate as replacement of sand at different percentages. When the samples were exposed to 200 °C, the mean mass variation was within a range of 5.95% to 6.86%. Similar trend can be seen for all the temperatures, such as for 400 °C, the variation was 7.44% to 8.52%, for 600 °C the variation was 9.77% to 10.61% and for 800 °C the mass variation was within a range of 10.54% to 11.21%. Fig. 10 also shows that, with the use of FNS aggregate, the mass loss fluctuated for 25% to 75% sand replacements. However, the mortar samples with 100% FNS aggregate (PC-FNS100) consistently exhibited a higher mass loss in all four temperature stages. This marginally higher mass loss of mortar with 100% FNS aggregate is considered to be associated with the higher moisture content of FNS aggregate.

3.5.3 Strength loss after exposure to high temperature

Compressive strength of the specimens was determined after the elevated temperature exposure and the percentage residual strength was calculated relative to the 28-day compressive strength of unheated samples. The residual strength percentages after exposure to different temperatures are shown in Fig. 16. It is noticeable that there was no strength loss of the control mortar (PC-FNS0) after exposure to 200 °C.

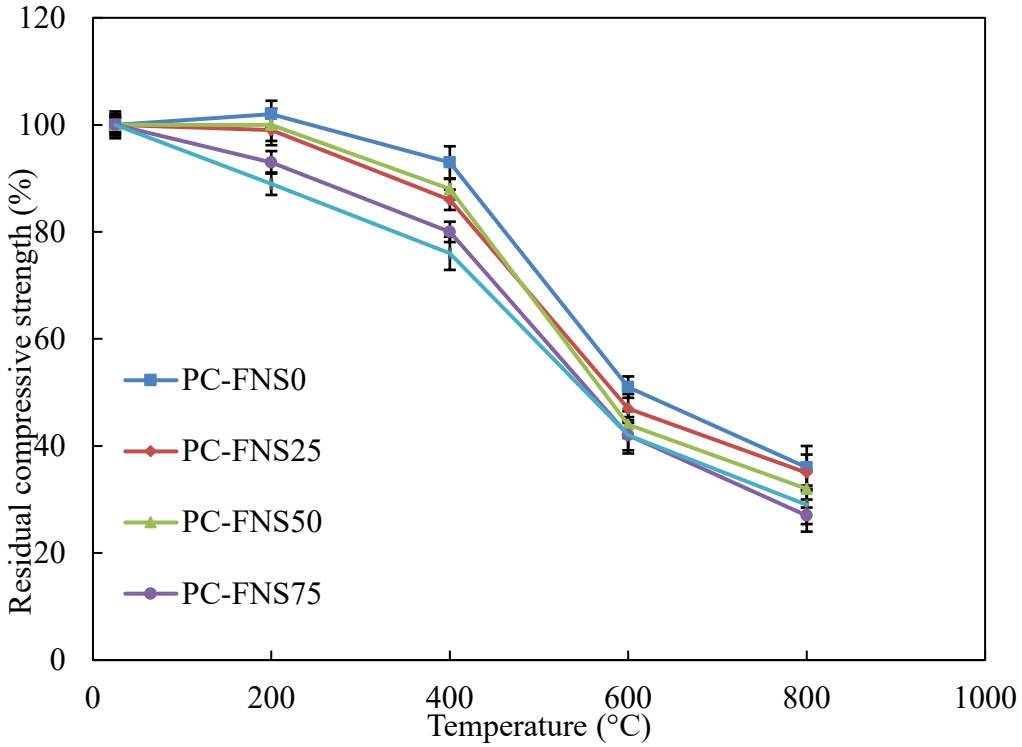

Fig. 16. Residual strength after exposure to different elevated temperatures.

However, replacement of sand by FNS aggregate gradually reduced the residual strength of mortar. Residual strengths of the specimens PC-FNS25, PC-FNS50, PC-FNS75 and PC-FNS100 were 99%, 100%, 93% and 89%, respectively. Furthermore, there was a gradual reduction of compressive strength from 200 to 400 °C for all the five mortar specimens. The residual compressive strengths of specimens PC-FNS0, PC-FNS25, PC-FNS50, PC-FNS75 and PC-FNS100 were 93%, 86%, 88%, 80% and 76%, respectively. With the increase of exposure temperature to 600 °C, the specimens exhibited considerable strength loss with residual compressive strengths within a range of 42% to 51%. The control mortar specimen, PC-FNS0 exhibited the highest residual strength and the samples with 100% FNS aggregates, PC-FNS100 exhibited the lowest residual strength. This noticeable reduction of residual strength at this temperature was primarily due to the decomposition of portlandite. The residual strength of the samples were 51%, 47%, 44%, 42% and 42% for PC-FNS0, PC-FNS25, PC-FNS50, PC-FNS75 and PC-FNS100, respectively. Finally, after exposure to 800 °C, the residual strengths of the samples were within a range of 27% to 36%. Thus, the results indicate that the residual strength of mortar marginally declined with the increase of FNS aggregate. Previous studies on concrete with high-density aggregates exhibited significantly high strength loss and explosive spalling due to elevated temperature exposure (Ma et al., 2015). However, no spalling was observed in the mortar specimens containing FNS aggregate. This phenomenon

457 is attributed to the higher VPV of the samples containing FNS aggregate that helped with the
458 release of vapour pressure. Therefore, even though high density FNS aggregates were used in
459 the mortar specimens exposed to elevated temperature, only marginal strength reduction was
460 observed due to their higher porosity, low thermal conductivity and thermal diffusivity, which
461 were observed in previous sections.

462 **4. Conclusions**

463 By-product ferronickel slag (FNS) was used in cement mortar as replacement of natural sand
464 at different percentages. The effects of FNS on compressive strength, volume of permeable
465 voids (VPV), thermal properties and residual strength after exposure to high temperature were
466 studied. The following conclusions are drawn from the experimental results.

467 1. Compressive strength of mortar increased for using 25% and 50% FNS aggregates and then
468 declined for 75% and 100% FNS aggregate. The change in strength by FNS is attributed to its
469 effect on the mortar density and overall grading of fine aggregate.

470 2. Density of mortar increased by FNS aggregate due to its higher particle density. Also,
471 porosity or VPV of mortar increased with the increase of FNS due to its large cavity and
472 micropores, angular shape and larger size than sand.

473 3. Thermal conductivity and thermal diffusivity of mortar decreased with the increase of FNS
474 content due to the increase of porosity. The decreases of thermal conductivity for using 50%
475 and 100% FNS were 30% and 50%, respectively. The increase of FNS content increased the
476 heat capacity of mortar. Thus, the thermal insulating properties and thermal mass of mortar
477 improved by use of FNS aggregate.

478 4. The residual strength of mortar after prolonged exposure to 600 ºC decreased from 51% for
479 using 0% FNS to 42% for 100% FNS. Similarly, the residual strengths decreased from 36%
480 for 0% FNS to 27% for 100% FNS after exposure to 800 ºC. The marginally higher strength
481 loss for using FNS aggregate is attributed to the decrease of thermal conductivity and
482 diffusivity.

483 5. Overall, FNS aggregate improved the thermal insulating properties of cement mortar without
484 sacrificing compressive strength. This can provide considerable benefits to the heating and
485 cooling energy usage of buildings. Thus, FNS aggregate has the potential for practical
486 applications in construction of energy efficient sustainable building products. Future trend
487 would be investigation of the long term durability of mortar using FNS aggregate.

488

489 **Acknowledgements**

490 The authors would like to acknowledge the support of SLN, New Caledonia through its
491 research department. Part of this research was undertaken using the EM instrumentation (ARC
492 LE130100053) at the John de Laeter Centre, Curtin University.

493 **References**

494 Alengaram, U. J., Al Muhit, B. A., bin Jumaat, M. Z., & Jing, M. L. Y. (2013). A comparison
495 of the thermal conductivity of oil palm shell foamed concrete with conventional
496 materials. Materials & Design, 51, 522-529.

497 Andrews-Phaedonos, F. (2008, July). Test methods for the assessment of durability of concrete.
498 In ARRB conference, 23rd, 2008, Adelaide, South Australia, Australia.

499 AS 2701 (2001). Methods of sampling and testing mortar for masonry construction. Standards
500 Australia, Sydney, Australia.

501 AS 2758.1 (2014). Aggregates and rock for engineering purposes Part 1: Concrete aggregates.
502 Standards Australia, Sydney, Australia.

503 Ashworth, T., and Ashworth, E., in: Graves, R.S., and Wysocki, D.C. (Eds.). Insulation
504 Materials: Testing and Applications. Vol. 1116, ASTM STP, Philadelphia, 1991, 415 –
505 429.

506 Berman, R. (1956). Some experiments on thermal contact at low temperatures. J. Applied
507 Physics, 27(4), 318-323.

508 Bogas, J. A., de Brito, J., & Figueiredo, J. M. (2015). Mechanical characterization of concrete
509 produced with recycled lightweight expanded clay aggregate concrete. Journal of
510 Cleaner Production, 89, 187-195.

511 Borinaga-Trevino, R., Pascual-Munoz, P., Castro-Fresno, D., & Del Coz-Díaz, J. J. (2013).
512 Study of different grouting materials used in vertical geothermal closed-loop heat
513 exchangers. Applied Thermal Engineering, 50(1), 159-167.

514 Bouduerra, A., Laurent, J.P., Goual, M.S., and Queneudec, M. (1997). The measurement of the
515 thermal conductivity of solid aggregates using the transient plane source technique.
516 Journal of Physics D: Applied Physics, 30, 2900-2904.

517 Del Coz Díaz, J. J., Rabanal, F. P. Á., Nieto, P. J. G., Hernández, J. D., Soria, B. R., & Pérez-
518 Bella, J. M. (2013). Hygrothermal properties of lightweight concrete: Experiments and
519 numerical fitting study. Construction and Building Materials, 40, 543-555.

520 Del Coz Díaz, J. J., Nieto, P. G., Hernández, J. D., & Rabanal, F. Á. (2010). A FEM
521 comparative analysis of the thermal efficiency among floors made up of clay, concrete
522 and lightweight concrete hollow blocks. Applied Thermal Engineering, 30(17-18),
523 2822-2826.

524 Demirboga, R., & Kan, A. (2012). Thermal conductivity and shrinkage properties of modified
525 waste polystyrene aggregate concretes. Construction and Building Materials, 35, 730-
526 734.

527 Emborg, M. (2014). Thermal stresses in concrete at early ages. In Analysis of concrete
528 structures by fracture mechanics (pp. 74-89). CRC Press.

529 Esteves, L. P. (2011). On the hydration of water-entrained cement–silica systems: combined
530 SEM, XRD and thermal analysis in cement pastes. Thermochimica Acta, 518(1-2), 27-
531 35.

532 Fu, X., & Chung, D. D. L. (1997). Effects of silica fume, latex, methylcellulose, and carbon
533 fibers on the thermal conductivity and specific heat of cement paste. Cement and
534 concrete research, 27(12), 1799-1804.

535 Gustafsson, S. E. (1991) Transient plane source techniques for thermal conductivity and
536 thermal diffusivity measurements of solid materials. Review of Scientific Instruments,
537 62, 797. doi: 10.1063/1.1142087

538 Gustafsson, S. E., Karawaski, E., Chohan, M. A. (1986). Thermal transport studies of
539 electrically conducting materials using the transient hot-strip technique. J. Phys. D:
540 Applied Physics, 19, 727-735.

541 Güneyisi, E., Gesoglu, M., Ghanim, H., İpek, S., & Taha, I. (2016). Influence of the artificial
542 lightweight aggregate on fresh properties and compressive strength of the self-
543 compacting mortars. Construction and Building Materials, 116, 151-158.

544 Ghods, P., Alizadeh, R., Salehi, M. (2017). Electrical methods and systems for concrete testing,
545 United States patent US 9, 638, 652. https://www.google.com/patents/ US9638652.

546 Institution of Structural Engineers, Concrete Society. (1987). Guide to the Structural Use of
547 Lightweight Aggregate Concrete, I. Struct. E, London, 58p.

548 Kodur, V. (2014). Properties of concrete at elevated temperatures. ISRN Civil engineering,
549 2014.

550 Kodur, V. K. R., & Sultan, M. A. (2003). Effect of temperature on thermal properties of high-
551 strength concrete. Journal of materials in civil engineering, 15(2), 101-107.

552 Kodur, V. K. R., Cheng, F. P., Wang, T. C., & Sultan, M. A. (2003). Effect of strength and
553 fiber reinforcement on fire resistance of high-strength concrete columns. Journal of
554 Structural Engineering, 129(2), 253-259.

555 Kong, D. L., & Sanjayan, J. G. (2010). Effect of elevated temperatures on geopolymer paste,
556 mortar and concrete. Cement and concrete research, 40(2), 334-339.

557 Kim, H. K., Jeon, J. H., & Lee, H. K. (2012). Workability, and mechanical, acoustic and
558 thermal properties of lightweight aggregate concrete with a high volume of entrained
559 air. Construction and Building Materials, 29, 193-200.

560 Li, Z., Xu, J., & Bai, E. (2012). Static and dynamic mechanical properties of concrete after
561 high temperature exposure. Materials Science and Engineering: A, 544, 27-32.

562 Lightfoot, E.N., Bird, R.B., Stewart, W.E. (1960). Transport Phenomena. John Wiley and Sons,
563 780p.

564 Liu, M. Y. J., Alengaram, U. J., Jumaat, M. Z., & Mo, K. H. (2014). Evaluation of thermal
565 conductivity, mechanical and transport properties of lightweight aggregate foamed
566 geopolymer concrete. Energy and Buildings, 72, 238-245.

567 Mahlia, T. M. I., Taufiq, B. N., & Masjuki, H. H. (2007). Correlation between thermal
568 conductivity and the thickness of selected insulation materials for building wall. Energy
569 and Buildings, 39(2), 182-187.

570 Ma, Q., Guo, R., Zhao, Z., Lin, Z., & He, K. (2015). Mechanical properties of concrete at high
571 temperature—a review. Construction and Building Materials, 93, 371-383.

572 Metha, K. P., & Monteiro, P. J. M. (2006). Concrete Microstructure, Properties, and Materials
573 (third ed.), McGraw-Hill, University of California at Berkeley

574 Mirzazadeh, M. M., Noël, M., & Green, M. F. (2016). Effects of low temperature on the static
575 behaviour of reinforced concrete beams with temperature differentials. Construction
576 and Building Materials, 112, 191-201.

577 Morabito, P. (1989). Measurement of the thermal properties of different concretes. High
578 Temperatures. High Pressures, 21(1), 51-59.

579 Örüng, I. (1996). A research on usage possibilities of ground lightweight aggregate in
580 agricultural buildings. Atatürk üniversitesi Ziraat fakultesi Dergisi, Turkey, 26(1).

581 Padmalal, D., Maya, K., Sreebha, S., & Sreeja, R. (2008). Environmental effects of river sand
582 mining: a case from the river catchments of Vembanad lake, Southwest coast of India.
583 Environmental geology, 54(4), 879-889.

584 Papayianni, I., & Valliasis, T. (2005). Heat deformations of fly ash concrete. Cement and
585 Concrete Composites, 27(2), 249-254.

586 Pan, Z., Sanjayan, J. G., & Kong, D. L. (2012). Effect of aggregate size on spalling of
587 geopolymer and Portland cement concretes subjected to elevated temperatures.
588 Construction and Building Materials, 36, 365-372.

589 Preciso, E., Salemi, E., & Billi, P. (2012). Land use changes, torrent control works and
590 sediment mining: effects on channel morphology and sediment flux, case study of the
591 Reno River (Northern Italy). Hydrological Processes, 26(8), 1134-1148.

592 Ramírez, F. M. D., Muñoz, F. B., López, E. L., & Polanco, A. V. (2013). Thermal evaluation
593 of structural concretes for construction of biodigesters. Energy and Buildings, 58, 310-
594 318.

595 Resnick, R. and Halliday, D. (1966) Physics. John Wiley and Sons, 1334p.

596 Saha, A. K., & Sarker, P. K. (2017a). Sustainable use of ferronickel slag fine aggregate and fly
597 ash in structural concrete: mechanical properties and leaching study. Journal of Cleaner
598 Production, 162, 438-448.

599 Saha, A. K., & Sarker, P. K. (2017b). Durability characteristics of concrete using ferronickel
600 slag fine aggregate and fly ash. Magazine of Concrete Research, 1-10.

601 Saha, A. K., & Sarker, P. K. (2017c). Compressive strength of mortar containing ferronickel
602 slag as replacement of natural sand. Procedia engineering, 171, 689-694.

603 Saha, A. K., & Sarker, P. K. (2018a). Durability of Mortar Incorporating Ferronickel Slag
604 Aggregate and Supplementary Cementitious Materials Subjected to Wet–Dry Cycles.
605 International Journal of Concrete Structures and Materials, 12(1), 29.

606 Saha, A. K., & Sarker, P. K. (2018b). Potential ASR expansion mitigation of ferronickel slag
607 aggregate by fly ash. Structural Concrete. DOI:10.1002/suco.201700273 (in press).

608 Saha, A. K. (2018). Effect of class F fly ash on the durability properties of concrete. Sustainable
609 Environment Research, 28(1), 25-31.

610 Saha, A. K., Khan, M. N. N., & Sarker, P. K. (2018). Value added utilization of by-product
611 electric furnace ferronickel slag as construction materials: A review. Resources,
612 Conservation and Recycling, 134, 10-24.

613 Saha, A. K., & Sarker, P. K. (2016). Expansion due to alkali-silica reaction of ferronickel slag
614 fine aggregate in OPC and blended cement mortars. Construction and Building
615 Materials, 123, 135-142.

616 Sayadi, A. A., Tapia, J. V., Neitzert, T. R., & Clifton, G. C. (2016). Effects of expanded
617 polystyrene (EPS) particles on fire resistance, thermal conductivity and compressive
618 strength of foamed concrete. Construction and building materials, 112, 716-724.

619 Sengul, O., Azizi, S., Karaosmanoglu, F., & Tasdemir, M. A. (2011). Effect of expanded perlite
620 on the mechanical properties and thermal conductivity of lightweight concrete. Energy
621 and Buildings, 43(2-3), 671-676.

622 Smili, B., Messaoud, A., Bouchelaghem, W., Abadlia, L., Fazel, N., Benmoussa, A., Kaban,
623 I., Gasser, F., & Gasser, J. G. (2018). Temperature dependence of the electrical
624 resistivity and absolute thermoelectric power of amorphous metallic glass Ni33. 3Zr66.
625 7. Journal of Non-Crystalline Solids, 481, 352-360.

626 Shen, D., Jiang, J., Shen, J., Yao, P., & Jiang, G. (2016). Influence of curing temperature on
627 autogenous shrinkage and cracking resistance of high-performance concrete at an early
628 age. Construction and Building Materials, 103, 67-76.

629 Soleimanzadeh, S., & Mydin, M. O. (2012). Influence of high temperatures on flexural strength
630 of foamed concrete containing fly ash and polypropylene fiber. International Journal of
631 Engineering-Transactions B: Applications, 26(2), 117.

632 Steiger, R.V., and Hurd, M.K. (1978). Lightweight insulating concrete for floors and roof
633 decks. Concrete Constructions, 23(7), 411-422.

634 Thomas, T. R., Probert, S. D. (1970). Thermal contact resistance: the directional effect and
635 other problems. Int. J. of Heat and Mass Transfer, 13(5), 789-807.

636 United States Environmental Protection Agency (US EPA). (2009). Hazardous waste
637 characteristics. Available at: www.epa.gov/sites/production/files/2016-
638 01/documents/hw-char.pdf (Accessed on 15 May 2015).

639 Williamson, M., Majumdar, R. (1992). Effect of surface deformations on contact conductance.
640 Journal of Heat Transfer, 114, 802-810.

641 Won, J. P., Kang, H. B., Lee, S. J., Lee, S. W., & Kang, J. W. (2011). Thermal characteristics
642 of high-strength polymer–cement composites with lightweight aggregates and
643 polypropylene fiber. Construction and Building Materials, 25(10), 3810-3819.

644 Yüzer, N., Aköz, F., & Öztürk, L. D. (2004). Compressive strength–color change relation in
645 mortars at high temperature. Cement and Concrete Research, 34(10), 1803-1807.

646 Yun, T. S., Jeong, Y. J., Han, T. S., & Youm, K. S. (2013). Evaluation of thermal conductivity
647 for thermally insulated concretes. Energy and Buildings, 61, 125-132.

648 Zhang, B., Bicanic, N., Pearce, C. J., & Balabanic, G. (2000). Residual fracture properties of
649 normal-and high-strength concrete subject to elevated temperatures. Magazine of
650 Concrete Research, 52(2), 123-136.